

Article citation info:

Al-Haddad A L, Giernacki W, Shandookh A. A, Abdulhady Jaber A, Puchalski R, Vibration Signal Processing for Multirotor UAVs Fault Diagnosis: Filtering or Multiresolution Analysis?, *Eksploracja i Niezawodność – Maintenance and Reliability* 2024; 26(1) <http://doi.org/10.17531/ein/176318>

Vibration Signal Processing for Multirotor UAVs Fault Diagnosis: Filtering or Multiresolution Analysis?

Indexed by:



Lutfi A. Al-Haddad^a, Wojciech Giernacki^b, Ahmed A. Shandookh^c, Alaa Abdulhady Jaber^c, Radosław Puchalski^{b,*}

^a Training and Workshops Center, University Of Technology- Iraq, Iraq

^b Faculty of Automatic Control, Robotics and Electrical Engineering, Institute of Robotics and Machine Intelligence, Poznan University of Technology, Poland

^c Mechanical Engineering Department, University of Technology- Iraq, Iraq

Highlights

- Comprehensive evaluation of Kalman filtering and DWT in UAV fault diagnosis.
- Experimental setup includes vibration accelerometer and data acquisition system.
- Finite element analysis determines optimal 1024 Hz sampling frequency.
- DWT outperforms Kalman filtering in revealing intricate fault details.
- Study contributes to state-of-the-art in multirotor UAV health monitoring.

Abstract

In the modern technological advancements, Unmanned Aerial Vehicles (UAVs) have emerged across diverse applications. As UAVs evolve, fault diagnosis witnessed great advancements, with signal processing methodologies taking center stage. This paper presents an assessment of vibration-based signal processing techniques, focusing on Kalman filtering (KF) and Discrete Wavelet Transform (DWT) multiresolution analysis. Experimental evaluation of healthy and faulty states in a quadcopter, using an accelerometer, are presented. The determination of the 1024 Hz sampling frequency is facilitated through finite element analysis of 20 mode shapes. KF exhibits commendable performance, successfully segregating faulty and healthy peaks within an acceptable range. While the six-level multi-decomposition unveils good explanations for fluctuations eluding KF. Ultimately, both KF and DWT showcase high-performance capabilities in fault diagnosis. However, DWT shows superior assessment precision, uncovering intricate details and facilitating a holistic understanding of fault-related characteristics.

Keywords

signal processing, fast fourier transform, discrete wavelet transform, kalman filter, UAVs

This is an open access article under the CC BY license (<https://creativecommons.org/licenses/by/4.0/>)

1. Introduction

The widespread use of UAVs has revolutionized a variety of industries and altered the way we approach crucial tasks over the past decade. Commonly known as drones, these adaptable and nimble aircraft have applications in a wide range of industries [1–4], from the military and surveillance [5, 6] to agriculture [7], environmental monitoring [8–11], and delivery

services [12]. The proliferation of UAVs has substantially improved the effectiveness and safety of numerous domains. Farmers utilize UAVs endowed with sophisticated sensors to monitor crop health, optimize irrigation, and apply targeted fertilizers, resulting in increased yields and decreased resource waste. In the logistics industry, drones have been effectively

(*) Corresponding author.

E-mail addresses:

L. A. Al-Haddad (ORCID: 0000-0001-7832-1048) lutfi.a.alhaddad@uotechnology.edu.iq,

W. Giernacki (ORCID: 0000-0003-1747-4010) wojciech.giernacki@put.poznan.pl, A. A. Shandookh (ORCID: 0000-0003-3729-704X)

ahmed.a.shandookh@uotechnology.edu.iq, A. Abdulhady Jaber (ORCID: 0000-0001-5709-195X) alaa.a.jaber@uotechnology.edu.iq,

R. Puchalski (ORCID: 0000-0002-5535-4442) radoslaw.puchalski@doctorate.put.poznan.pl

implemented for expedient and cost-effective last-mile deliveries, particularly in remote and inaccessible areas. As UAVs became increasingly prevalent in various industries, the demand for robust and dependable systems increases. The emergence of fault diagnosis methodologies is attributable to the inherent risk of UAVs experiencing operational malfunctions [13]. The potential repercussions of a UAV failure, whether caused by a technical malfunction or an external disturbance, emphasized the need for proactive measures to detect and resolve defects prior to their escalation into critical incidents. Fault diagnosis methodologies include sensor data analysis [14], machine learning algorithms [15, 16], and redundancy design in order to perpetually monitor the UAV's health and performance [17, 18]. By recognizing anomalies, predicting potential problems, and enabling timely maintenance or adaptive control procedures, these fault detection methodologies have played a crucial role in enhancing the safety, reliability, and efficiency of UAV operations, thereby fostering the widespread acceptance and integration of UAVs across a variety of applications.

Fault diagnosis strategies for predictive maintenance is widely applicable [19, 20]. In the field of defect diagnosis for UAVs, although some may depend on different analyzing methods [21, 22], vibration signal analysis has arisen as a highly effective and extensively adopted technique [23]. During their operational lifetimes, the mechanical and structural components of UAVs are susceptible to wear, strain, and other forms of physical duress. Vibration signals are useful indicators of the condition and health of these components. By analyzing the vibrational patterns generated while navigation or as the UAV is in operation, scientists and technicians are able to identify subtle changes or irregularities that may indicate impending failures. Analysis of vibration signals enables the early detection of problems, allowing for proactive maintenance and preventing potentially catastrophic occurrences. This technique improves the UAV's dependability and endurance while also contributing to the safety of the UAV, its payload, and the surrounding environment. UAV operators may benefit from improved fault identification capabilities by continually improving and integrating vibration signal analysis methods, resulting in safer and more efficient UAV operations across a broad variety of applications. It is now extensively used in

UAV defect diagnostics because to the ubiquity of vibration signals in high-speed rotating equipment. Among the mentioned methodologies lies the method of wavelet transform [24], and the spectrum analysis approach [25].

Kalman filtering is a powerful estimating technique used to iteratively estimate the state of a dynamic system from a sequence of noisy measurements in terms of signal filtering techniques. It combines real-time sensor readings with predictions from a mathematical model of the system's behavior to provide an optimum estimate of the system's state [26, 27]. By combining data from various onboard sensors, such as GPS, accelerometers, and gyroscopes, Kalman filters play a crucial role in enhancing the navigation and control precision of UAVs [28, 29]. Kalman filters facilitate high accuracy flight path planning and autonomous navigation, which are extremely essential for the success of UAV operations [30, 31]. Moreover, Kalman filtering has proved useful for UAV fault diagnosis [32]. They can detect anomalies and deviations caused by defects in the UAV's mechanical, electrical, or propulsion mechanisms by integrating data from multiple sensors and comparing it to the expected behavior of the UAV model [33]. Because of its ability to handle chaotic data and account for uncertainties, the filter is a suitable tool for finding and isolating problems, leading to enhanced UAV safety and reliability. Kalman filters offer rapid and appropriate reactions to possible issues by delivering diagnostic information in real time, permitting timely maintenance activities and reducing delay. Consequently, the application of Kalman filtering in UAV fault diagnosis has become a crucial aspect of assuring the sustained success and efficacy of UAV missions in a variety of industries [34]. In [35], a study was conducted to examine the dependability of several sensor types in the context of real-time vibration-based anomaly inspection in drones. The vibration signals underwent filtration utilizing a Kalman filter-based processing technique in order to get an uncluttered and undisturbed visual representation.

In terms of multiresolution analysis, FFT (Fast Fourier Transform) [36, 37] signal processing has proved to be a valuable technique for UAV fault diagnosis [38]. In this context, FFT is used to analyze vibration signals recorded during operation from various UAV components. FFT enables engineers to identify specific frequency components associated with normal and aberrant behavior by transforming time-

domain vibration data into the frequency domain [39]. This helps in the detection of potential flaws or irregularities in the UAV's mechanical and structural systems, allowing for timely maintenance and mitigating the risk of catastrophic failures. Spectrum analysis based on FFT [40] was utilized to discriminate between the operational frequencies on a trimotor [41]. The states of healthy and damaged blade of a quadcopter are studied based on signal processing in real-time decision-making process [42]. However, sophisticated techniques such as Continuous Wavelet Transform (CWT) [43, 44] and Discrete Wavelet Transform (DWT) [45–48] have been employed to further improve fault diagnosis capabilities. These multiresolution analysis techniques provide a more comprehensive analysis of the vibration signals. CWT provides a continuous scale representation, enabling the identification of transitory or time-varying frequencies, while DWT decomposes the signals into various scales and offers both time and frequency localization. Engineers can extract fine-grained features and obtain a deeper understanding of the UAV's performance by utilizing CWT and DWT. This facilitates the detection of subtle variations and concealed patterns that would otherwise go undetected by conventional FFT. The combination of FFT, CWT, and DWT in UAV fault diagnosis guarantees a comprehensive comprehension of the UAV's health, which leads to more accurate diagnostics and proactive maintenance strategies, thereby ensuring more secure and dependable UAV operations across a variety of applications. In addition, when combined with machine learning techniques [49, 50], DWT can provide accurate and efficient fault diagnosis results.

There is a notable research deficiency in the field of UAV fault detection and maintenance pertaining to the most effective method for analyzing vibration signals in multirotor UAVs. The use of vibration signal analysis has gained significant popularity, although the decision between conventional filtering techniques and more sophisticated multiresolution analysis approaches, such as CWT and DWT, remains a topic of ongoing investigation. In order to bridge this existing knowledge gap, the objective of this research article is to examine and contrast the effectiveness of these two distinct signal processing methodologies that have been particularly designed for multirotor UAVs. The originality of this study comes in conducting a full assessment of vibration signal

processing procedures within the particular context of UAVs and directly comparing the effectiveness of filtering and multiresolution analysis techniques. Through a comprehensive assessment of the merits and constraints associated with each methodology, significant and important perspectives are furnished to provide guidance to operators and maintenance employees of UAVs in order to facilitate informed decision-making pertaining to the most appropriate technique for diagnosing faults in UAVs. This study aims to provide a comprehensive analysis of vibration signal processing methodologies, with the objective of improving the safety, reliability, and efficiency of multirotor UAV operations in many sectors.

The paper's structure continues as follows: section 2 elucidates the fundamental concepts of both discrete wavelet transform and Kalman filter. Section 3 expounds on the experimental setup and methodology of the proposed data calculation approach, incorporating a block diagram illustrating the implementation of the two methods. In section 4, the study's outcomes are presented and critically analyzed with the aid of figures and supportive evidence, enabling a comparative assessment of the effectiveness of each signal processing technique for UAV fault diagnosis. Finally, the paper culminates with section 5, which succinctly synthesizes the principal findings and their implications. The research's workflow diagram is visually depicted in Figure 1 to offer a clear representation of the investigation's progression.

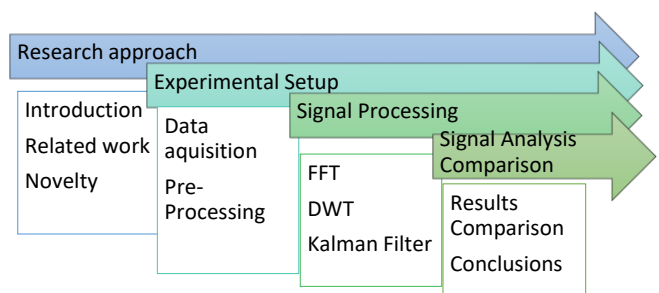


Fig. 1. The research workflow diagram.

2. Theoretical Basis

2.1. Fast Fourier Transform-Based Wavelet Transform Levels

The FFT is a popular algorithm for computing the discrete Fourier transform of an order or time-domain signal. It was first introduced in the mid-1960s [51]. In order to analyze the

frequency components of a signal, the discrete Fourier transform converts it from the time domain to the frequency domain. The FFT significantly accelerates this computation process contrasted to the standard discrete Fourier transform, particularly for large datasets, making it a fundamental instrument in a variety of disciplines, such as signal processing, image processing, communication networks, processing of audio, and more [52]. The FFT algorithm divides the calculation into smaller subproblems and uses symmetries to reduce the number of required computations, resulting in a substantial increase in efficiency and performance. It has evolved into a must-have tool for analyzing and processing digital data in a broad range of practical applications. The process can be done by dividing a signal $x(t)$ into sinusoidal components of unlimited temporal period [53], provided by equation 1:

$$x(w) = \int_{-\infty}^{\infty} x(t)e^{-j\omega t} dt \quad (1)$$

Where t represents time, w is the radian frequency, and $x(w)$ is the signal transformed. In addition to that, it should be noted that frequency-domain-based analysis is heavily utilized in vibration analysis [54], especially those vibration signals acquired from quadcopter drones for the outcome of fault diagnosis [42].

2.2. Discrete Wavelet Transform

The Discrete Wavelet Transform (DWT) is a mathematical approach that is commonly utilized in signal processing and data reduction. Decomposing a given signal into a group of wavelets is accomplished by scaling and translation of a basic wavelet known as the mother wavelet. The signal is hierarchically broken down into various levels as a result of this recursive approach. The DWT has a number of benefits over other signal processing approaches, including the ability to appropriately represent signals with rapid variations and the effective use of computing and memory resources. The DWT's fundamental strength is its ability to do multi-resolution analysis, allowing the signal to be broken into separate frequency elements with varied degrees of accuracy.

In the wavelet series analysis, the methodology starts by selecting a main mother wavelet to be aligned with the analyzed signal. The selection of the optimal mother wavelet has a significant impact on the analysis of precision and accuracy. Mother wavelets serve as the fundamental functions for

decomposing the input signal into distinct frequency components and capturing its characteristics at multiple scales. Different mother wavelets have special properties, such as frequency localization, vanishing moments, and regularity, that would make them suitable for specific signal categories or use. The choosing of the mother wavelet should be based on the characteristics of the signal under analysis and the application's requirements. Commonly used mother wavelets include Daubechies, Haar, Symlets, Coiflets, and Morlet, each of which has its own benefits and drawbacks [55, 56]. The selection process requires balancing the trade-offs between time and frequency localization, computational complexity, and the ability to accurately depict signal features, making it essential to accomplish the desired level of signal analysis and compression within the context of the DWT. Selecting the optimal mother wavelet ensures an efficient and informative DWT analysis, which facilitates the extraction of pertinent data and improves the performance of various signal processing tasks. Daubechies' fourth order (db4) will be employed in this research article [50]. Figure 2 depicts the analysis wavelet and scaling of the db4 as well as the synthesis wavelet and scaling.

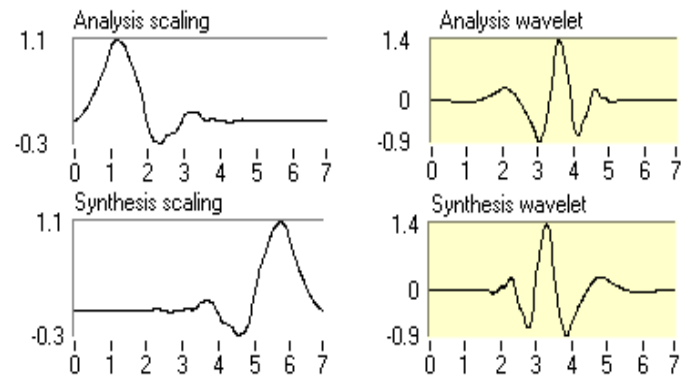


Fig. 2. Analysis and synthesis of Daubechies order 4 (db4) mother wavelet.

Subsequently, the computed inner product represents the continuous wavelet transform (CWT) coefficients between the analyzed signal and a set of daughter wavelets. These daughter wavelets are derived from the original mother wavelet $\Psi(t)$ through a combination of scaling (s) and shifting (n) operations. The scaling and shifting parameters enable the modification of the daughter wavelets in terms of their size and position, providing a flexible and adaptive representation of different features within the signal. In the shifting step, the wavelet is successively translated along the X-axis until it fully covers the

entire investigated signal. Mathematically, the CWT coefficient $WT(n, s)$ is obtained by computing the integral of the product between the input signal $x(t)$ and the translated and scaled version of the mother wavelet $\Psi\left(\frac{t-n}{s}\right)$, with $\frac{1}{\sqrt{s}}$ serving as a normalization factor. This process enables the extraction of time-frequency information from the signal, revealing its spectral characteristics at different scales and positions as following in equation 2 [57]:

$$WT(n, s) = \frac{1}{\sqrt{s}} \int_{-\infty}^{+\infty} x(t) \Psi\left(\frac{t-n}{s}\right) dt \quad (2)$$

The CWT provides more precision in signal processing; however, it is potentially endlessly redundant, resulting in a significant amount of irrelevant information and making it unsustainable [58]. The DWT was developed to address this issue by only scaling and altering the main mother wavelet at discrete points, making it more efficient and practical for many applications. The DWT decomposes the signal into several signals with defined frequency bandwidths that can be analyzed individually. It uses filters with multiple cut-off frequencies to evaluate the data at different scales and create a time-scale representation of the signal. In general, a multi-resolution analysis in several frequency bands with variable resolutions may be accomplished by subdividing time-domain signals using the DWT [59]. $cD1[k]$ and $cA1[k]$ represent the DWT coefficients at the first level of decomposition, a crucial phase in wavelet analysis. In this context, the DWT permits the decomposition of a discrete signal, represented by $x[n]$, into two sets of coefficients: $cD1[k]$ representing the high-frequency or detail subband information, and $cA1[k]$

representing the low-frequency or approximation subband components. The process entails convolving the input signal with high-pass and low-pass filter coefficients and aggregating the results over various shift values (n). This shifting and scaling operation efficiently extracts the signal's localized frequency components. $cD1[k]$ encapsulates high-frequency information, such as rapid variations or edges, whereas $cA1[k]$ captures the signal's low-frequency components and overall trends. These coefficients provide a compact and meaningful representation of the original signal in the frequency domain, enabling a multi-resolution analysis and facilitating a number of signal processing tasks, including denoising, compression, and feature extraction. This can be mathematically interoperated as demonstrated in equations 3 and 4 [60]:

$$cD1[k] = \sum_n x[n] * h * [2k - n] \quad (3)$$

$$cA1[k] = \sum_n x[n] * g * [2k - n] \quad (4)$$

or, by rewriting the equations above that show the first level of decomposition, into equations that show the l level of decomposition. In this research, six level decomposition will be utilized in equations 5 and 6 below.

$$cD_l[k] = \sum_n cD_{l-1}[n] * h * [2k - n] \quad (5)$$

$$cA_l[k] = \sum_n cA_{l-1}[n] * g * [2k - n] \quad (6)$$

To further understand the process of DWT's decomposition, Figure 3 elaborates the procedure. The low pass filters keep going into high pass and low pass filters, until a certain desired level of decomposition is achieved. In this work, a six-level decomposition is adopted whereas the frequency range is to be explained in the next experimental validation section.

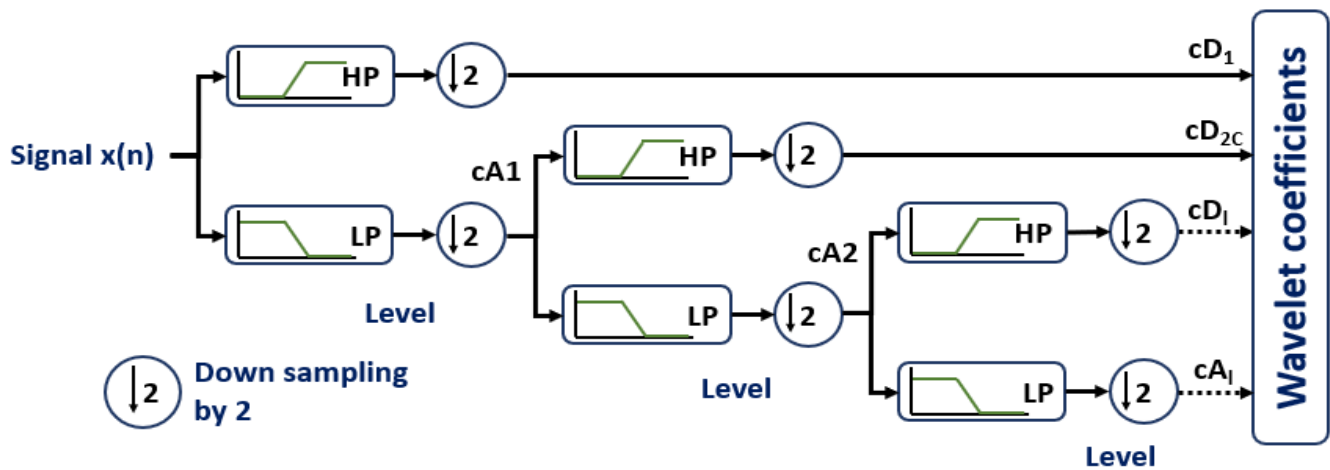


Fig. 3. Signal decomposition of multi-levels employing DWT [50].

After decomposing a signal with the DWT technique, a set of coefficients representing the various frequency components of the original signal at various levels or scales is obtained. To entirely reconstruct the original signal from its decomposed components, signal synthesis is required. Signal synthesis, also known as wavelet reconstruction, is the process of regenerating the original signal by combining the DWT coefficients acquired during decomposition. Reconstructing the signal from its detail and approximation coefficients at each level employs the inverse discrete wavelet transform (IDWT). The IDWT combines the frequency bands of the coefficients by applying

the conjugates of the filters used in the decomposition procedure, which are the inverse filters as described in Figure 4 below. Signal synthesis allows us to recover the original signal with minimal information loss, assuming that the decomposition and synthesis procedures are precisely implemented. This reconstruction is essential in applications where the original signal must be restored after processing in the wavelet domain. It ensures that the insights obtained from the decomposition of frequency components can be utilized effectively for the analysis and processing of the original signal.

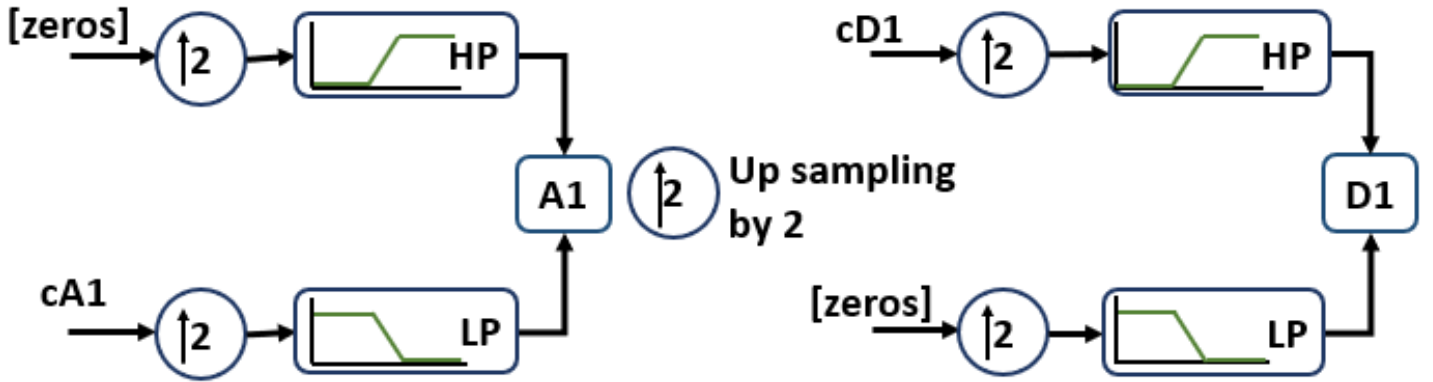


Fig. 4. The process of reconstructing the approximation and detail signals through the utilization of zero padding [50].

2.3. Kalman Filter-based Signal Processing

Kalman filters are repetitive mathematical techniques used for the purpose of achieving optimum estimation and state forecasting for dynamic systems. These filters integrate past knowledge with real-time data to provide accurate and effective estimates of the system's state. The implementation of a Kalman filter is often used to mitigate the impact of noise present in raw sensor readings. This is achieved by adaptively altering the current sensor measurement using previous sensor data. In this particular instance, the Kalman filtering technique was only employed to process the unprocessed data outputs of the utilized ADXL335 vibration sensor, despite the absence of significant noise seen from this sensor in comparison with other accelerometers. The Kalman filter may be mathematically represented by the following 7 and 8 set of equations [35]:

$$x_k = Ax_{k-1} + Bu_{k-1} + w_k \quad (7)$$

$$z_k = Hx_k + v_k \quad (8)$$

Where the vectors x , z , and u are representing the state, measurement or observation, and feedback vectors, accordingly.

The state transition matrix A is responsible for establishing the correlation between the state at time step $k - 1$ and the state at step k . On the other hand, the feedback matrix B is responsible for establishing the connection between the control input u and the state x . In contrast, the measurement matrix H establishes a connection between the state x_k and the measurement z_k . The variables w_k and v_k represent the process and measurement noises, respectively. These variables are used to account for random disturbances and uncertainties that impact the development of the state and the measurement process. The Kalman filter method may be categorized into two distinct algorithms: state prediction, also known as time update, and correction, sometimes referred to as measurement update. The technique used for state prediction is based upon the subsequent equations numbered 9 and 10 [35]:

$$\hat{x}_k^- = A\hat{x}_{k-1} + Bu_{k-1} \quad (9)$$

$$P_k^- = AP_{k-1}A^T + Q \quad (10)$$

The variable \hat{x}_k^- represents the previous state, which is calculated prior to the adjustment made during the measurement update. On the other hand, P_k^- denotes the prior covariance

matrix. The symbol Q is used to denote the matrix representing the covariance of process noise. The adjustment algorithms are formally specified as follows [35]:

$$K_k = P_k^- H^T (H P_k^- H^T + R)^{-1} \quad (11)$$

$$\hat{x}_k = \hat{x}_k^- + K_k (z_k - H \hat{x}_k^-) \quad (12)$$

$$P_k = (I - K_k H) P_k^- \quad (13)$$

In the Kalman filtering adjustment process, various parameters play crucial roles, namely the Kalman gain (K_k), the posteriori error covariance matrix (P_k), the covariance matrix of the measurement noise or filter deviation matrix (R), the estimate of the state vector (x) at time k (represented by \hat{x}_k , the optimum filter value), and the unit matrix (I). The Kalman filter continuously performs prediction and correction steps, enabling the generation of estimated measurement values and consequently reducing the impact of measurement noise present in the sensor system. In this study, measurements are obtained from the ADXL335 vibration sensor at a specific sampling frequency and a frequency resolution of 0.01 Hz, with a cut-off frequency within the range of [100-200] Hz.

3. Methodology

3.1. Experimental Validation

The experimental validation of the proposed methodology was conducted using a DJI Mini 2 combo drone [61–63], as illustrated in Figure 5. The experimental setup involved fixing the accelerometer at the center of the drone, precisely at the intersection of the actuators' cross lines forming an X mark. The drone's operation was controlled by the DJI control unit, with operating speed and height settings determined through a smartphone interface. The accelerometer, with specifications detailed in Table 1, was interfaced with a data acquisition system whose specifications are characterized in Table 2. The acquired signal was further processed using a high-performance Lenovo Core i7 laptop functioning as the central processing unit. The dedicated signal processing program, detailed in the forthcoming section, facilitated the comprehensive analysis of the recorded data. The carefully designed experimental setup ensures accurate and precise data collection, enabling a rigorous investigation of the proposed fault diagnosis methodology's performance and efficacy.

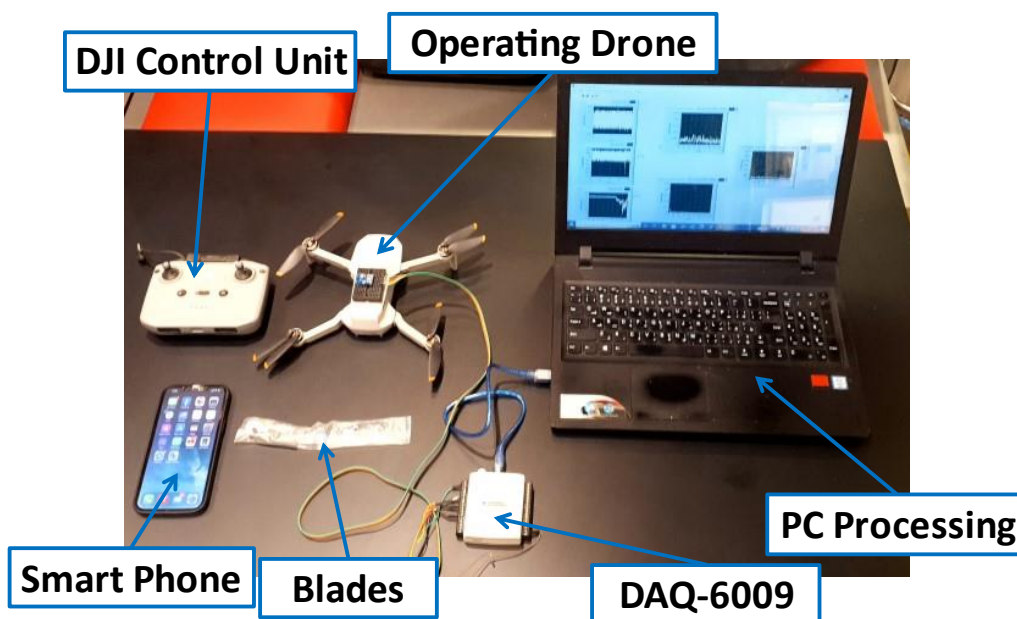


Fig. 5. Experimental tools for experiment progressing.

Table 1. ADXL335 vibration accelerometer parametrical values.

No.	General Specification	Information
1	Operating voltage	5 V
2	Sensitivity	300 mV/g
3	Bandwidth	X and Y axes: 0.5-1600 Hz; Z axes: 0.5-550 Hz
4	Full-scale range	+/- 3 g

Table 2. DAQ-6009 parametrical values.

No.	General Specification	Information
1	Dimensions without connectors	.63.5 mm × 85.1 mm × 23.2 mm
2	Weight With connectors	84 g
3	Analog Input (AI) resolution	14 bits differential, 13 bits single-ended
4	Maximum AI sample rate	48 kS/s

In order to investigate the impact of damage on the drone, a specific location of the blade was selected for introduction of the fault. The choice of the lower left blade was made randomly to simulate a fault scenario, enabling the acquisition of distinct vibration patterns representing both the healthy and faulty states as listed in Table 3. The spatial location of this chosen blade is depicted in Figure 6a, wherein a top view schematic of the multirotor UAV is presented. To properly position the accelerometer, a coordinate system was established: the X-axis represents a centerline traversing from the top to the bottom of the drone, while the Y-axis is defined by the opposite direction of the X-axis. The Z-axis, being orthogonal to the page, is also depicted in Figure 6a. In contrast, the drone undergoes pitching motion about the Y-axis, rolling motion around the X-axis, and yawing motion against the Z-axis. For simulating the induced

faults, Figure 6b illustrates the mass removal of 0.5 grams from the overall weight of the drone, which initially weighed 249 grams. Moreover, the drone is going to operate in hover mode where the actuator speed is around 10,000 RPM and hence 168 Hz with a height above sea level of 1.2 m. The healthy drone, undergoes a mass removal from one of its blades, inducing an unbalance pattern in the actuators and leading to vibration of the damaged blades, ultimately resulting in a full structural vibration of the quadcopter. These vibration patterns are recorded through the accelerometer and subsequently interpreted as vibration signals using LabVIEW software [64, 65]. The experimental design and methodology adopted in this investigation ensure the controlled introduction of faults, facilitating the comprehensive analysis of the drone's dynamic behavior and vibration characteristics.

Table 3. Studied cases.

Case	Hovering Speed (RPM)	Hovering Speed (Hz)	Height From Ground (m)	Location of Damaged Blade	Drone Weight When Operating (Kgs)
Healthy	10,000	168	1.2	N/A	0.249
Faulty	10,000	168	1.2	As specified in Figure 6	0.2485

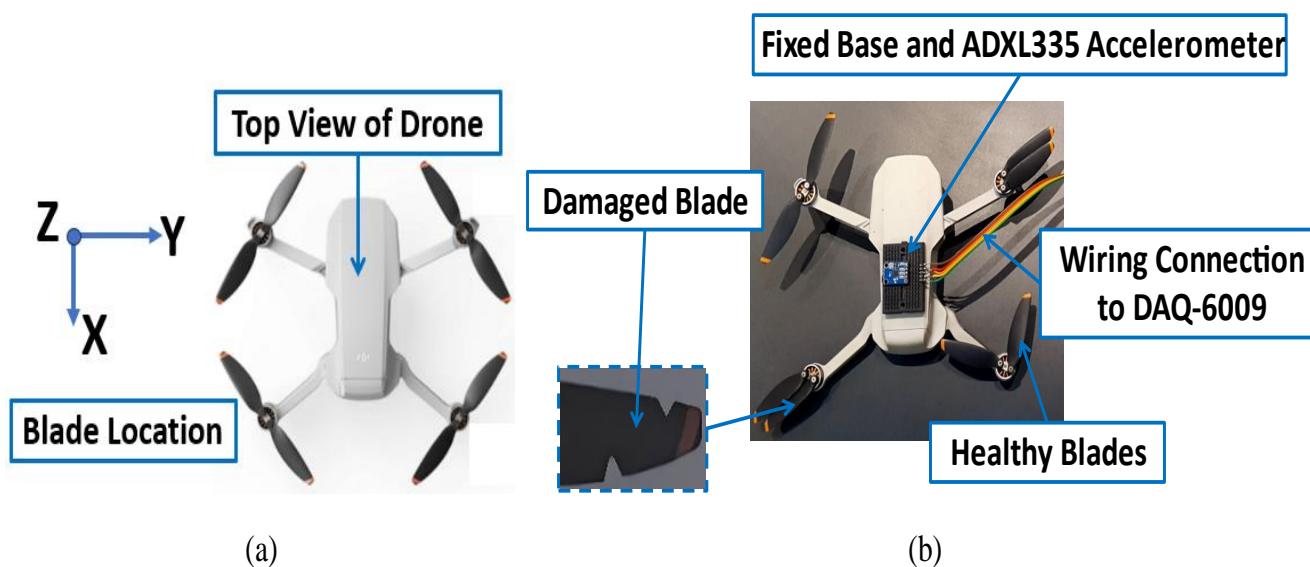


Fig. 6. Damage introduction and vibration measurement: (a) Location of the damaged blade and the axis of operation; (b) Induced damage and accelerometer position.

3.2. Finite Element Analysis Approach

In engineering and applied sciences, Finite Element Analysis (FEA) is of paramount importance, serving as a potent computational tool for simulating and analyzing complex structures and systems [66–68]. FEA has made a great contribution to UAV analysis due to their capability of structural analyzing, design, and topology optimization [38, 69, 70]. This study employed FEA to determine the natural frequency of which the optimal sampling frequency for vibration signal acquisition will depend upon. The paper also aims to calculate and study the dynamic behavior and natural frequencies of the UAV structure by using the modal simulation analysis through ANSYS. This will enable the identification of natural frequency components and aids in the selection of an optimal sampling frequency to ensure the acquisition of accurate and robust row vibration data. The ability of FEA to provide detailed insights into the structural behavior of UAVs is extremely effective, as it enables UAV technicians to improve the reliability, safety, and performance of these aircraft, thereby contributing to the

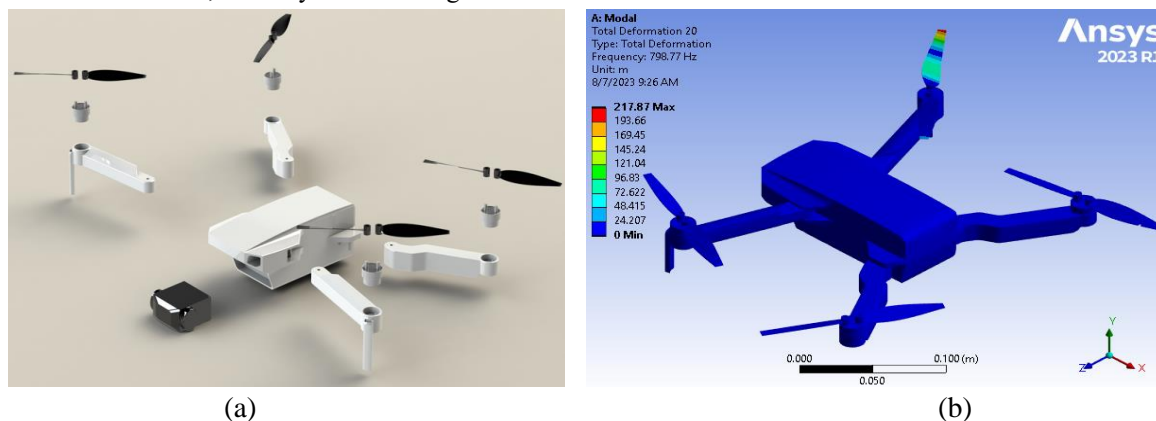


Fig. 7. Finite element analysis of the UAV drone: (a) Geometrical approach; (b) Final mode shape.

3.3. Signal Processing

In engineering and applied sciences, signal processing is essential because it processes signals to extract useful information and improve their quality [72]. Numerous methods, including filtering, transformation, feature extraction, and noise reduction, are used in it [73, 74]. Signal processing is essential for identifying patterns, anomalies, and trends in data gathered from mechanical systems like engines, turbines, and rotating gear when it comes to vibration signal analysis. By using sophisticated signal processing algorithms, researchers and engineers may effectively identify any malfunctions, provide diagnoses, and keep an eye on the functionality and well-being

advancement and integration of UAV technology for a wide range of applications.

The presented research used a mode simulation technique with 20 different mode shapes reflecting deformations in millimeters. This process needs only the natural frequency to include faults in the simulation, which is especially the case when talking about LabVIEW sample rate. Figure 7a shows the geometrical model of DJI drone used in this study which was assembled as indicated by the building requirements. Furthermore, Figure 7b displays natural frequency for a last mode shape, at 798.77 Hz. Consequently, it was realized that sampling rate should cover the last natural frequency and thus set over 800 Hz so as to ensure comprehensive data collection and analysis [71]. The modal simulation method is very important in understanding how drones behave structurally and their dynamic features thereby helping ascertain an appropriate as well as accurate sampling frequency that can be used according to need of the device regarding vibration signal analysis or UAVs' operational requirements.

of systems. As a result, preventive maintenance is made easier and catastrophic failures are avoided.

Signal processing techniques improve the precision, dependability, and efficacy of vibration signal analysis, which contributes significantly to the overall safety and operational efficacy of numerous industrial applications and essential machinery. In this research, Figure 8 depicts a block diagram of a system for calculating the vibration data of a drone in hover mode using Kalman filtering. A data acquisition (DAQ) assistant, a discrete Kalman filter, a spectral measurement block, and a write to measurement file block are included in the system. At a specified sampling rate of 1024 readings per 0.5 second,

the DAQ assistant collects vibration data from the drone's sensors. The discrete Kalman filter then estimates the vibration data using a cut off frequency of a range [100-200] Hz because the drone is going to operate in hovering speed of 168 Hz per

actuator. The RMS and phase of the vibration data are computed by the spectral measurement block, which can be used to analyze the vibration data. The write to measurement file block stores vibration data in a file, which can then be analyzed further.

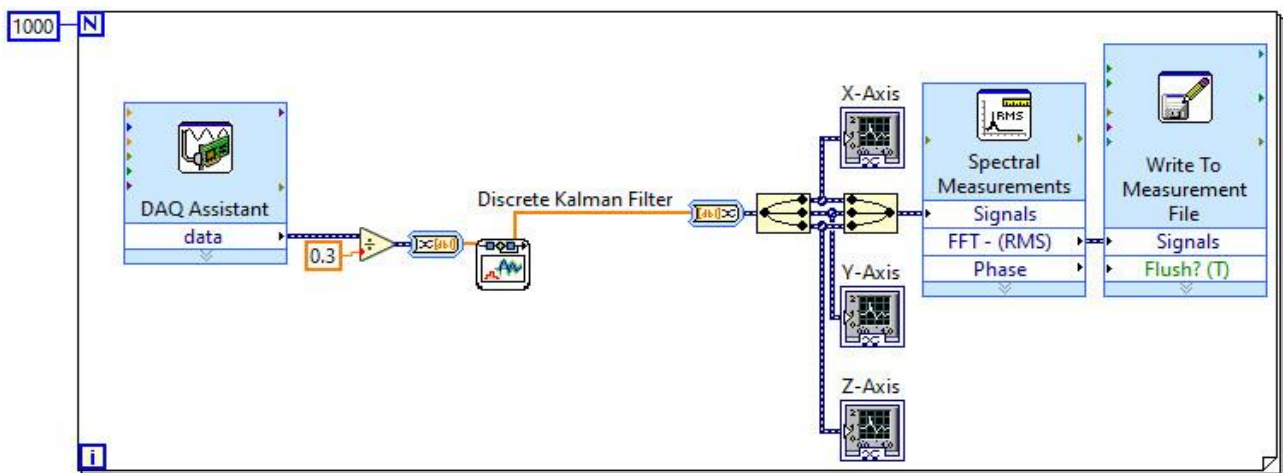


Fig. 8. A sample from the overall code and block diagram for Kalman filtering.

In contrast, the utilization of multiresolution analysis through DWT is demonstrated in the block diagram presented in Figure 9. In this approach, a six-level decomposition is employed, which enhances signal clarity and resolution. To ensure accurate representation of frequency content, the Nyquist frequency [71, 75] is taken into account, with the highest operating frequency (200 Hz) being multiplied by a factor of 2 (resulting in 400 Hz). A higher multiplication value, such as $(200 \times 5 = 1000 \text{ Hz})$, further improves frequency resolution. For that, and because the earlier natural frequency acquired from FEA, the sampling frequency is set to 1024 Hz. The six-level decomposition is tabulated in Table 4 for signal analysis purposes. Both the Kalman-filter-based signals and DWT-based signals undergo spectral analysis using FFT to

assess the effectiveness of removing unwanted random vibration signals. Additionally, to maintain constant calibration, a constant subtraction is applied to the input signals acquired from the ADXL335 accelerometer. This constant subtraction ensures signal calibration by subtracting the mean of the signals, corresponding to the static acceleration, thus enabling the use of only dynamic acceleration in terms of gravitational units (g). This calibration step enhances the accuracy and reliability of the subsequent signal processing and analysis, particularly in the context of vibration signal interpretation and fault diagnosis. The mean equation is expressed mathematically in equation 14 as:

$$AM = \frac{1}{N} \sum_{i=1}^N X_i \quad (14)$$

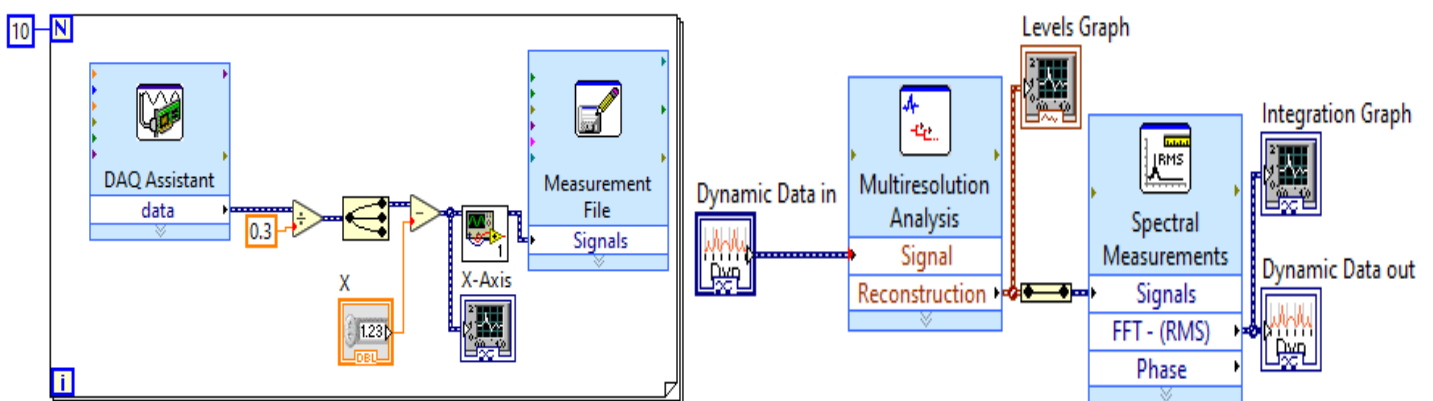


Fig. 9. A sample from the overall code and block diagram for multiresolution analysis.

Table 4. DWT Leveling frequency.

Decomposing Stages	1	2	3	4	5	6	Approx
Range of Frequency (Hz)	1024 – 512	512 – 256	256 – 128	128 – 64	64 – 32	32 – 16	16 – 0

4. Results and discussion

4.1. Time-Domain Vibration Signals

Figure 10 below depicts the acceleration in g units of the adopted drone operating in hover mode presented in the previous methodology, with a focus on healthy and faulty time-domain signals prior to and following the application of Kalman filtering. The x-axis indicates time in seconds with a 1-second interval, whereas the y-axis indicates vibration in g units ranging from -1 to 1. The healthy time-domain signal is depicted in green at a sampling frequency range of [0-1024 Hz] on the figure's left side. The post-filtered signal is depicted in dark brown below the healthy signal. Analyzing the signal from a healthy drone reveals that its acceleration fluctuates over time, as expected due to external disturbances and operating conditions. However, the implementation of Kalman filtering in the frequency range [100-200 Hz] results in a significant reduction of noise interference and a more stable, smoother acceleration profile. The post-filtered signal provides a refined representation of the drone's acceleration, allowing for a more accurate analysis and interpretation of its hover mode performance.

In contrast, the flawed time-domain signal is depicted in red

on the right side of the healthy signal, also captured at a sampling frequency range of [0-1024 Hz]. The faulty signal exhibits more pronounced acceleration fluctuations than the healthy signal, indicating a higher level of vibration during hover mode. This elevated vibration in the defective drone could be caused by a number of interactions, prior to the vibration moving pattern from blade to arm and then to the body and structure of the drone. Even after applying Kalman filtering in the frequency range [100-200 Hz] to the erroneous signal, the post-filtered signal continues to exhibit elevated acceleration values. Although the filtering process reduces the drone's vibrations, it does not eliminate all sources of disturbance. This disparity in acceleration profiles between healthy and malfunctioning drones suggests a discernible difference in vibration patterns, indicating the uncertainty of Kalman filters. However, the filtering procedure marginally eliminates induced vibration and random disturbances, resulting in an acceleration profile that is more uniform and stable for the healthy drone signal. Despite Kalman filtering, the erroneous drone signal continues to exhibit higher acceleration values, indicating the presence of vibrations that may be indicative of potential mechanical/operational issues or filtering issues.

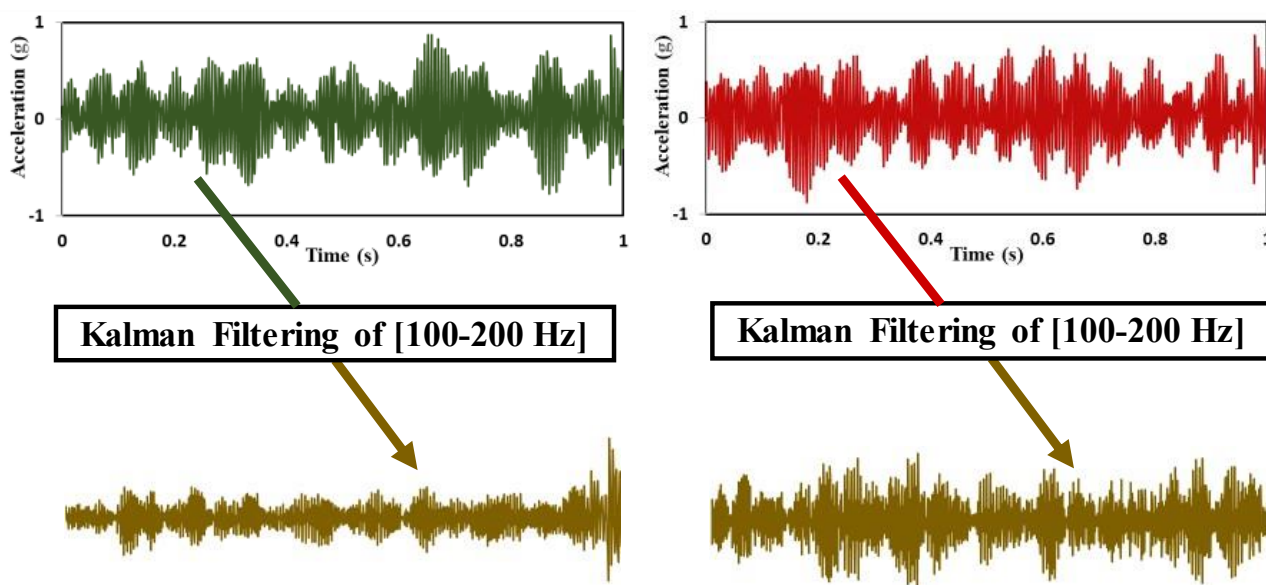


Fig. 10. Kalman filtering-based time-domain vibration signals of the operating drone.

The vibration signals from the same signal as in the previous graphs were decomposed into six levels, in addition to the approximation coefficient level, using the Discrete Wavelet Transform (DWT). Figure 11 presents the vibration signals for both healthy and faulty drone states, along with their respective six-level decompositions. Notably, levels 2 and 3 exhibit the highest signal fluctuation in terms of g unit vibrations when comparing the healthy and faulty drones, respectively. This phenomenon can be attributed to the fact that these two levels encompass the decomposed frequency range close to the drone's operating frequency during hovering at 168 Hz. Particularly, level 3 covers a frequency range from 128 Hz to 256 Hz. While

other levels provide supplementary insights, levels 2 and 3 not only isolate irrelevant random vibration signals but also offer meaningful interpretations of their underlying representations. For instance, wind speed may be associated with one of these levels, while the response to a faulty blade could correspond to another decomposition level. Further investigation involving mathematical modeling of additional physical components can establish the correspondence between vibration signals and their respective levels. Consequently, DWT demonstrates precision comparable to Kalman filtering in diagnosing faults in multirotor UAVs, while its capacity for enhanced explanations renders it a valuable diagnostic tool.

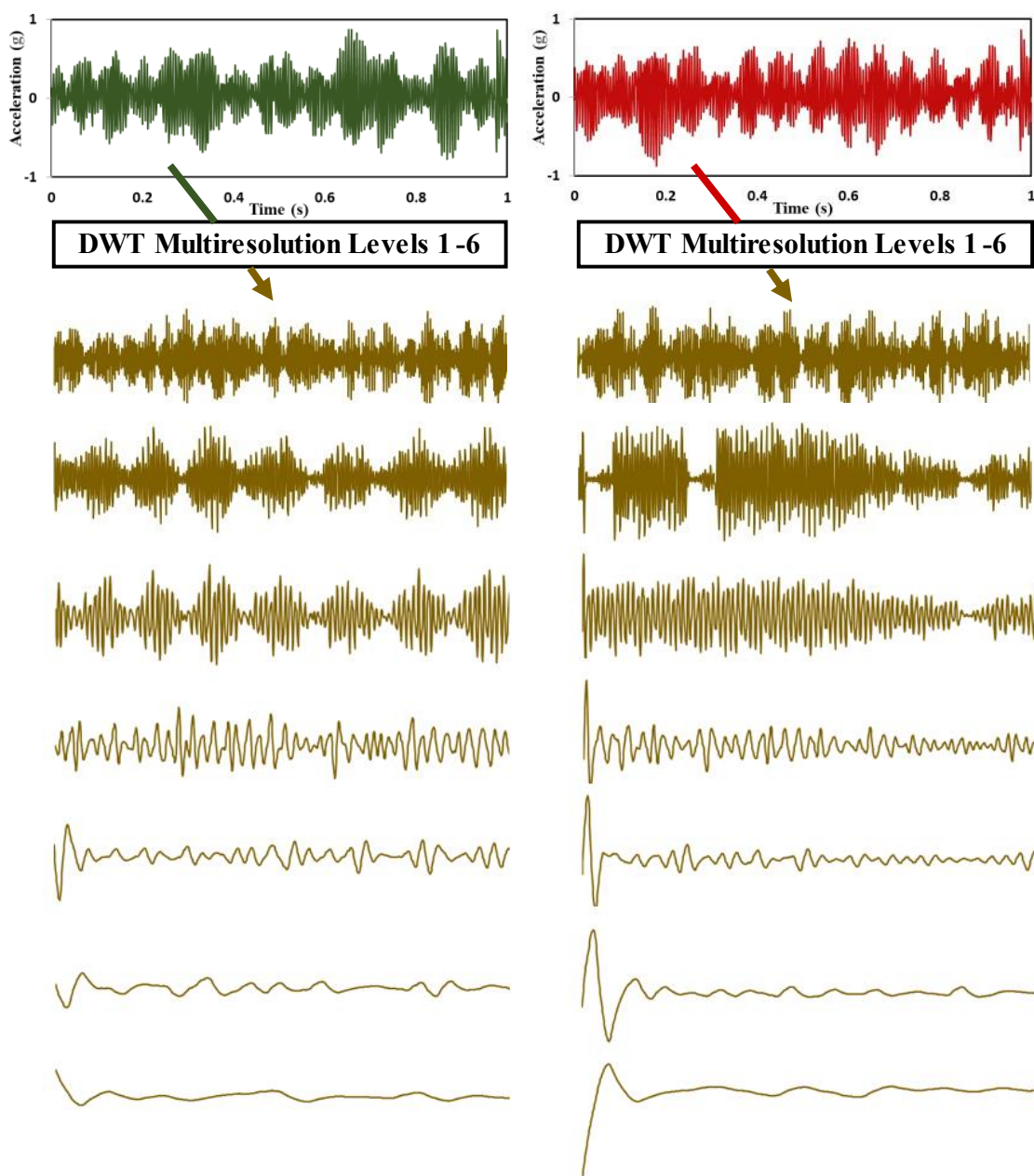


Fig. 11. DWT leveling-based time-domain vibration signals of the operating drone.

4.2. Frequency-Domain Vibration Signals

In the field of frequency-domain analysis, time-domain signals gain enhanced interpretability. This concept is exemplified through the presentation of Figure 12, which respectively illustrate Kalman filtered signals and their corresponding spectra under healthy and faulty operational conditions. A discernible observation in Figure 12a is the attenuation of amplitudes within the frequency range of [0 to 100] Hz following the application of filtering. This phenomenon is explicable by the adoption of Kalman filtering, which primarily captures amplitude fluctuations within a predefined frequency interval coinciding with the operational frequency. This facet

proves particularly advantageous for subsequent statistical feature extraction. Upon scrutinizing the spectral analysis of the faulty signal in Figure 12b, a notable deduction arises: the elimination of a peak at approximately 51 Hz. This frequency value potentially originates from the drone's actuator response aimed at stabilizing the system subsequent to the introduction of a blade fault. During Kalman filtering, this frequency component, lying beyond the designated frequency range, is consequently excluded from the spectral representation. This omission is unwarranted, given that such a frequency value could signify the presence of a fault, thereby emphasizing its relevance within the realm of fault diagnosis.

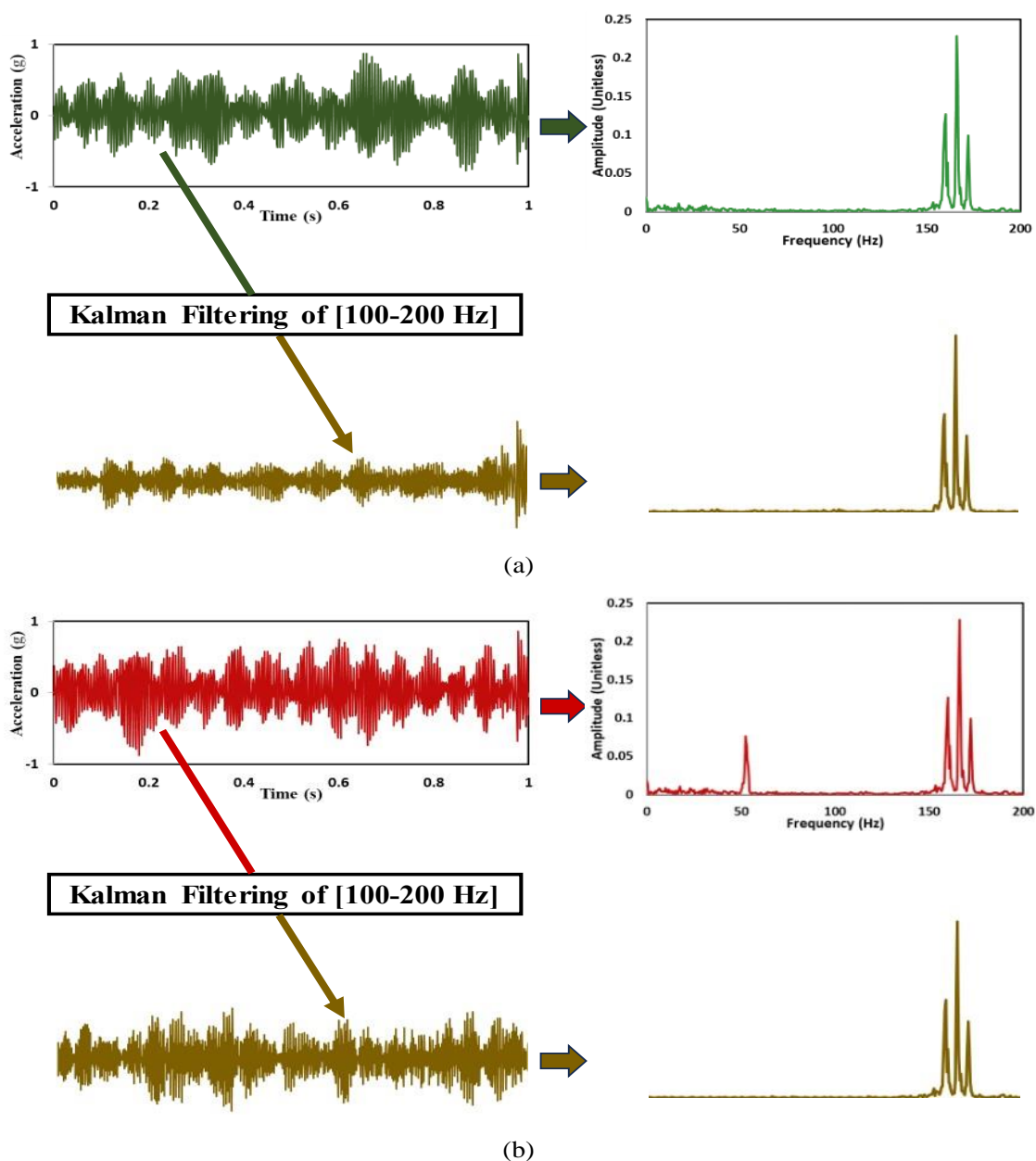


Fig. 12. Kalman filtering-based frequency-domain (a) healthy and (b) faulty vibration signals of the operating drone.

Consequently, the decomposed spectrum levels achieved through DWT are presented in Figures 13a and 13b, corresponding to the healthy and faulty operating modes, respectively. In Figure 13a, it is discernible that levels 2 and 3 exhibit the most pronounced impact, consistent with the observations detailed in subsection 4.1, wherein these levels manifested the highest amplitudes. Notably, a distinct frequency interval emerges within the range of 75 to 100 Hz, attributed to the actuators' propensity to counteract vibrational imbalances and restore drone equilibrium. Strikingly, this frequency interval remains imperceptible in the Kalman filtering-based signals, where the spectrum registers negligible amplitudes. Furthermore, the spectral analysis reveals three peaks within the 150 to 175 Hz range, discerningly partitioned across levels 2

and 3. Specifically, while two peaks manifest within level 2, the maximal peak, aligned with the operational frequency of 168 Hz, prominently emerges within level 3. Contrarily, the faulty operational decomposed levels, as depicted in Figure 13b, exhibit heightened fluctuations due to the compromised blade, inducing augmented vibrational dynamics in the drone's operation. A comparative examination of levels 2 and 3 distinctly unveils heightened amplitude fluctuations, unequivocally signifying the presence of faults or aberrant operational patterns. In summary, it can be inferred that the utilization of DWT-based analysis not only enhances the visual representation of signals, but also enables the efficient and reliable identification and utilization of operational frequencies.

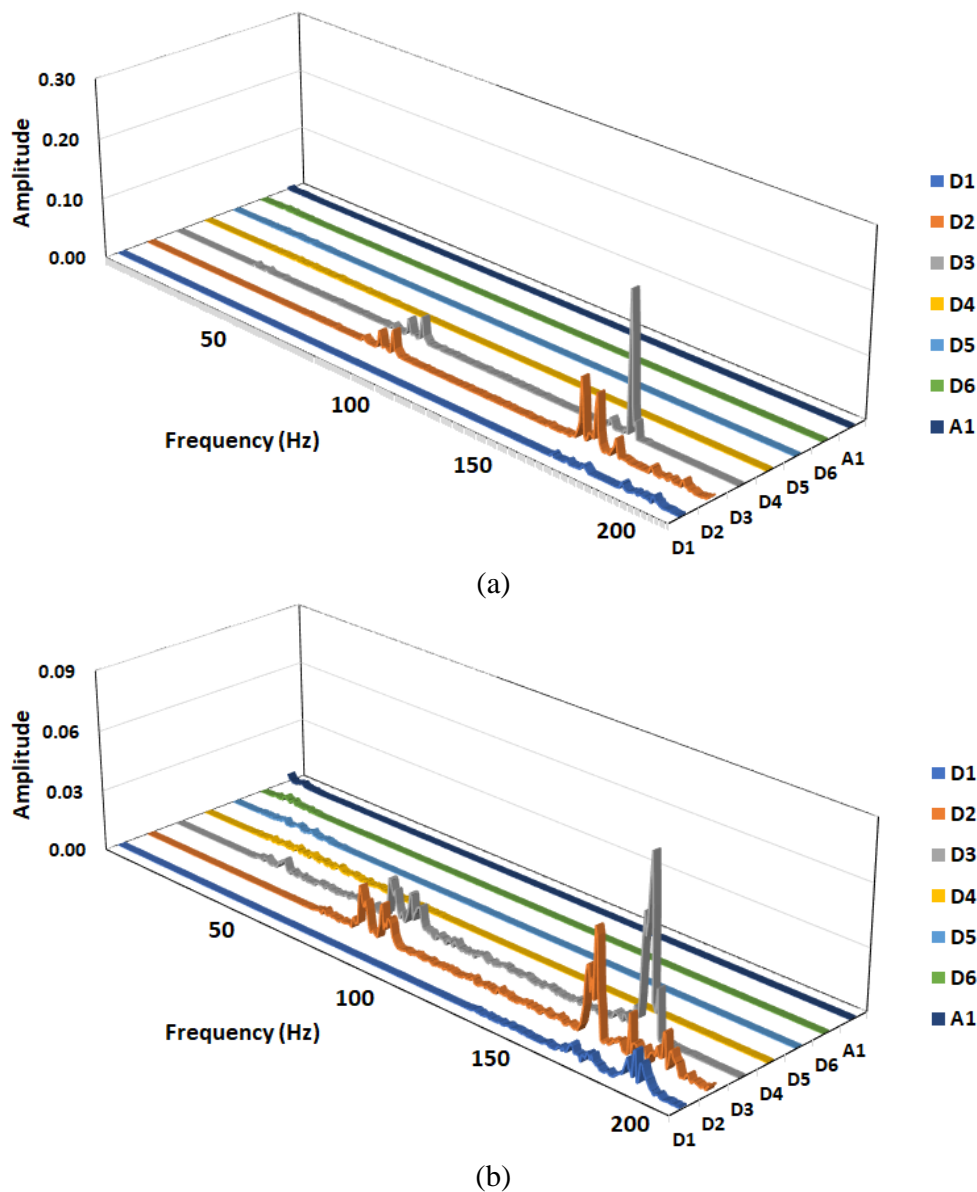


Fig. 13. DWT leveling-based frequency-domain vibration signals of the operating drone: (a) Healthy (b) Faulty.

This comparative analysis of two distinct approaches, namely Kalman filtering and DWT-based multiresolution analysis, has been conducted in the pursuit of effective fault diagnosis for multirotor UAVs. The presented results highlight the merits and limitations of each vibration signal processing methodology. The ability of Kalman filtering to reduce noise and improve signal stability contributes to the comprehension of operational patterns and disturbances. However, its efficacy is observed to vary in the presence of certain fault-related frequencies, which may result in missed fault indications. DWT-based multiresolution analysis, on the other hand, reveals a comprehensive perspective and provides detailed insights into signal components at various frequency levels. The ability to isolate particular frequency ranges improves diagnostic accuracy, especially when capturing fault-related patterns. In addition, DWT's proficiency in highlighting operational frequencies proves advantageous, as evidenced by the identification of relevant frequency intervals. The multiresolution analysis emerges as an advantageous method for fault diagnosis in multirotor UAVs, providing increased granularity and a broader frequency-domain perspective for improved reliability and precision in identifying faults and irregularities. In addition, this study's findings have practical implications for advancing fault diagnosis methodologies in multirotor UAVs. Utilizing the insights gained from Kalman filtering and DWT multiresolution analysis, practitioners can improve machine learning-based fault diagnosis by employing filtered vibration signals or concentrating on vibration signals derived from the most effective level of decomposition. These refined signals provide an exhaustive representation of operational characteristics and fault-related patterns, which can be translated into useful statistical features for training machine learning models. This application not only improves the precision of fault detection, but also contributes to the development of more robust and intelligent fault diagnosis systems for multirotor UAVs, enhancing their operational safety and reliability.

Funding

This work was supported by Poznan University of Technology grant no. 0214/SBAD/0241.

References

1. Milidonis, K., Eliades, A., Grigoriev, V., & Blanco, M. J. (2023). Unmanned Aerial Vehicles (UAVs) in the planning, operation and

5. Conclusion

In simplicity, this study employed an experimental approach to assess the processing of vibration signals in a quadcopter UAV during a stable state of hovering, with the actuator rotational speed held constant. The study employed Kalman filtering and DWT-based multiresolution analysis to capture vibration signals associated with both healthy and mass removal faults. The primary discoveries of this scholarly article are briefly outlined in the following:

- (1) Effective Fault Diagnosis Approaches: The study demonstrates the significance of signal processing methods, specifically Kalman filtering and DWT multiresolution analysis, for enhancing fault diagnosis accuracy in multirotor UAVs.
- (2) Experimental Validation: Through experimentation on healthy and faulty quadcopter operational states, utilizing vibration accelerometers and data acquisition systems, the study provides real-world insights into vibration signal analysis.
- (3) Kalman Filtering Strengths and Limitations: Kalman filtering effectively segregates faulty and healthy peaks in vibration signals, yet its capability to capture certain fault-related frequencies is limited.
- (4) DWT's Comprehensive Insight: Employing a six-level DWT multiresolution analysis, the study reveals intricate patterns within vibration signals, offering a deeper understanding of fault-related characteristics that may not be detected by Kalman filtering.
- (5) Future Perspectives and Contributions: The study concludes with insights into future research directions, emphasizing the invaluable contributions made to the current state-of-the-art in multirotor UAV fault diagnosis through enhanced signal processing methodologies, especially when progressed into machine learning methods.

- maintenance of concentrating solar thermal systems: A review. *Solar Energy*, 254, 182–194. <https://doi.org/https://doi.org/10.1016/j.solener.2023.03.005>
2. Cho, J., Lim, G., Biobaku, T., Kim, S., & Parsaei, H. (2015). Safety and Security Management with Unmanned Aerial Vehicle (UAV) in Oil and Gas Industry. *Procedia Manufacturing*, 3, 1343–1349. <https://doi.org/https://doi.org/10.1016/j.promfg.2015.07.290>
 3. Kim, D. H., Lee, B. K., & Sohn, S. Y. (2016). Quantifying technology–industry spillover effects based on patent citation network analysis of unmanned aerial vehicle (UAV). *Technological Forecasting and Social Change*, 105, 140–157. <https://doi.org/https://doi.org/10.1016/j.techfore.2016.01.025>
 4. Czyż, Z., Jakubczak, P., Podolak, P., Skiba, K., Karpiński, P., Drożdziel-Jurkiewicz, M., & Wendeker, M. (2023). Deformation measurement system for UAV components to improve their safe operation. *Eksploatacja i Niezawodność – Maintenance and Reliability*. <https://doi.org/10.17531/ein/172358>
 5. Hadi, H. J., Cao, Y., Nisa, K. U., Jamil, A. M., & Ni, Q. (2023). A comprehensive survey on security, privacy issues and emerging defence technologies for UAVs. *Journal of Network and Computer Applications*, 213, 103607. <https://doi.org/https://doi.org/10.1016/j.jnca.2023.103607>
 6. Kähler, S. T., Abben, T., Luna-Rodriguez, A., Tomat, M., & Jacobsen, T. (2022). An assessment of the acceptance and aesthetics of UAVs and helicopters through an experiment and a survey. *Technology in Society*, 71, 102096. <https://doi.org/https://doi.org/10.1016/j.techsoc.2022.102096>
 7. Amarasingam, N., Ashan Salgadoe, A. S., Powell, K., Gonzalez, L. F., & Natarajan, S. (2022). A review of UAV platforms, sensors, and applications for monitoring of sugarcane crops. *Remote Sensing Applications: Society and Environment*, 26, 100712. <https://doi.org/https://doi.org/10.1016/j.rsase.2022.100712>
 8. Saif, A., Dimiyati, K., Noordin, K. A., Mosali, N. A., G.C., D., & Alsamhi, S. H. (2023). Skyward bound: Empowering disaster resilience with multi-UAV-assisted B5G networks for enhanced connectivity and energy efficiency. *Internet of Things*, 100885. <https://doi.org/https://doi.org/10.1016/j.iot.2023.100885>
 9. Pecho, P., Škvareková, I., Ažaltovič, V., & Bugaj, M. (2019). UAV usage in the process of creating 3D maps by RGB spectrum. *Transportation Research Procedia*, 43, 328–333. <https://doi.org/https://doi.org/10.1016/j.trpro.2019.12.048>
 10. Asadzadeh, S., de Oliveira, W. J., & de Souza Filho, C. R. (2022). UAV-based remote sensing for the petroleum industry and environmental monitoring: State-of-the-art and perspectives. *Journal of Petroleum Science and Engineering*, 208, 109633. <https://doi.org/https://doi.org/10.1016/j.petrol.2021.109633>
 11. Sharma, R., & Arya, R. (2022). UAV based long range environment monitoring system with Industry 5.0 perspectives for smart city infrastructure. *Computers & Industrial Engineering*, 168, 108066. <https://doi.org/https://doi.org/10.1016/j.cie.2022.108066>
 12. Shen, B., Gu, Q., & Yang, G. (2023). Joint task offloading and UAVs deployment for UAV-assisted mobile edge computing. *Computer Networks*, 234, 109943. <https://doi.org/https://doi.org/10.1016/j.comnet.2023.109943>
 13. Puchalski, R., & Giernacki, W. (2022). UAV Fault Detection Methods, State-of-the-Art. *Drones*, 6(11), 330. <https://doi.org/10.3390/drones6110330>
 14. Saied, M., Mahairy, T., Francis, C., Shraim, H., Mazeh, H., & Rafei, M. El. (2019). Differential Flatness-Based Approach for Sensors and Actuators Fault Diagnosis of a Multirotor UAV. *IFAC-PapersOnLine*, 52(16), 831–836. <https://doi.org/https://doi.org/10.1016/j.ifacol.2019.12.066>
 15. T., T., Low, K. H., & Ng, B. F. (2023). Actuator fault detection and isolation on multi-rotor UAV using extreme learning neuro-fuzzy systems. *ISA Transactions*, 138, 168–185. <https://doi.org/https://doi.org/10.1016/j.isatra.2023.02.026>
 16. Liang, S., Zhang, S., Huang, Y., Zheng, X., Cheng, J., & Wu, S. (2022). Data-driven fault diagnosis of FW-UAVs with consideration of multiple operation conditions. *ISA Transactions*, 126, 472–485. <https://doi.org/https://doi.org/10.1016/j.isatra.2021.07.043>
 17. Li, Y., Zhu, X., & Yin, G. (2023). Robust actuator fault detection for quadrotor UAV with guaranteed sensitivity. *Control Engineering Practice*, 138, 105588. <https://doi.org/https://doi.org/10.1016/j.conengprac.2023.105588>
 18. Saied, M., Lussier, B., Fantoni, I., Shraim, H., & Francis, C. (2017). Fault Diagnosis and Fault-Tolerant Control of an Octorotor UAV using motors speeds measurements. *IFAC-PapersOnLine*, 50(1), 5263–5268. <https://doi.org/https://doi.org/10.1016/j.ifacol.2017.08.468>
 19. Su, S., Sun, Y., Peng, C., & Wang, Y. (2023). Aircraft Bleed Air System Fault Prediction based on Encoder-Decoder with Attention

- Mechanism. *Eksploracja i Niezawodność – Maintenance and Reliability*, 25(3). <https://doi.org/10.17531/ein/167792>
20. Zuber, N., & Bajrić, R. (2020). Gearbox faults feature selection and severity classification using machine learning. *Eksploracja i Niezawodność – Maintenance and Reliability*, 22(4), 748–756. <https://doi.org/10.17531/ein.2020.4.19>
 21. Jeon, S., Kang, J., Kim, J., & Cha, H. (2023). Detecting structural anomalies of quadcopter UAVs based on LSTM autoencoder. *Pervasive and Mobile Computing*, 88, 101736. <https://doi.org/https://doi.org/10.1016/j.pmcj.2022.101736>
 22. Yaman, O., Yol, F., & Altınors, A. (2022). A Fault Detection Method Based on Embedded Feature Extraction and SVM Classification for UAV Motors. *Microprocessors and Microsystems*, 94, 104683. <https://doi.org/https://doi.org/10.1016/j.micpro.2022.104683>
 23. Al-Haddad, L. A., & Jaber, A. (2022). Applications of Machine Learning Techniques for Fault Diagnosis of UAVs.
 24. Jaber, A. A., & Bicker, R. (2018). Development of a condition monitoring algorithm for industrial robots based on artificial intelligence and signal processing techniques. *International Journal of Electrical and Computer Engineering*, 8(2), 996–1009. <https://doi.org/10.11591/ijece.v8i2.pp996-1009>
 25. Jawad, S., & Jaber, A. (2022). Bearings Health Monitoring Based on Frequency-Domain Vibration Signals Analysis. *Engineering and Technology Journal*, 41(1), 86–95. <https://doi.org/10.30684/etj.2022.131581.1043>
 26. Camestrini, C., Heil, T., Kosch, S., & Jossen, A. (2016). A comparative study and review of different Kalman filters by applying an enhanced validation method. *Journal of Energy Storage*, 8, 142–159. <https://doi.org/https://doi.org/10.1016/j.est.2016.10.004>
 27. Kumarappan, M. V., Kashyap, K. R. A., & Prakasam, P. (2023). Fused empirical mode decomposition with spectral flatness and adaptive filtering technique for denoising of ECG signals. *Analog Integrated Circuits and Signal Processing*, 114(1), 41–50. <https://doi.org/10.1007/s10470-022-02120-0>
 28. Zang, Y., Li, Y., Duan, Y., Li, X., Chang, X., & Li, Z. (2023). Event-triggered Extended Kalman Filter for UAV Monitoring System. In *2023 IEEE 12th Data Driven Control and Learning Systems Conference (DDCLS)* (pp. 2032–2036). <https://doi.org/10.1109/DDCLS58216.2023.10167412>
 29. Yan, D., Zhang, W., Chen, H., & Shi, J. (2023). Robust control strategy for multi-UAVs system using MPC combined with Kalman-consensus filter and disturbance observer. *ISA Transactions*, 135, 35–51. <https://doi.org/https://doi.org/10.1016/j.isatra.2022.09.021>
 30. Omotuyi, O., & Kumar, M. (2021). UAV Visual-Inertial Dynamics (VI-D) Odometry using Unscented Kalman Filter. *IFAC-PapersOnLine*, 54(20), 814–819. <https://doi.org/https://doi.org/10.1016/j.ifacol.2021.11.272>
 31. Wang, X., Guo, J., & Cui, N. (2009). Adaptive extended Kalman filtering applied to low-cost MEMS IMU/GPS integration for UAV. In *2009 International Conference on Mechatronics and Automation* (pp. 2214–2218). <https://doi.org/10.1109/ICMA.2009.5246654>
 32. Driessen, S. P. H., Janssen, N. H. J., Wang, L., Palmer, J. L., & Nijmeijer, H. (2018). Experimentally Validated Extended Kalman Filter for UAV State Estimation Using Low-Cost Sensors. *IFAC-PapersOnLine*, 51(15), 43–48. <https://doi.org/https://doi.org/10.1016/j.ifacol.2018.09.088>
 33. Benzerrouk, H., Nebylov, A., & Salhi, H. (2016). Quadrotor UAV state estimation based on High-Degree Cubature Kalman filter. *IFAC-PapersOnLine*, 49(17), 349–354. <https://doi.org/https://doi.org/10.1016/j.ifacol.2016.09.060>
 34. Kim, S.-H., Negash, L., & Choi, H.-L. (2016). Cubature Kalman Filter Based Fault Detection and Isolation for Formation Control of Multi-UAVs. *IFAC-PapersOnLine*, 49(15), 63–68. <https://doi.org/https://doi.org/10.1016/j.ifacol.2016.07.710>
 35. Ghazali, M. H. M., & Rahiman, W. (2022). An Investigation of the Reliability of Different Types of Sensors in the Real-Time Vibration-Based Anomaly Inspection in Drone. *Sensors*, 22(16). <https://doi.org/10.3390/s22166015>
 36. Bhandari, S., & Jotautienė, E. (2022). Vibration Analysis of a Roller Bearing Condition Used in a Tangential Threshing Drum of a Combine Harvester for the Smooth and Continuous Performance of Agricultural Crop Harvesting. *Agriculture (Switzerland)*, 12(11). <https://doi.org/10.3390/agriculture12111969>
 37. Sanjeet, S., Sahoo, B. D., & Parhi, K. K. (2023). Low-energy real FFT architectures and their applications to seizure prediction from EEG. *Analog Integrated Circuits and Signal Processing*, 114(3), 287–298. <https://doi.org/10.1007/s10470-022-02094-z>
 38. Al-Haddad, L. A., & Jaber, A. A. (2023). Influence of Operationally Consumed Propellers on Multirotor UAVs Airworthiness: Finite Element and Experimental Approach. *IEEE Sensors Journal*, 1. <https://doi.org/10.1109/JSEN.2023.3267043>
 39. Rebiai, M., Ould Zmirli, M., Bengherbia, B., & Lachenani, S. A. (2023). Faults Diagnosis of Rolling-Element Bearings Based on Fourier Decomposition Method and Teager Energy Operator. *Arabian Journal for Science and Engineering*, 48(5), 6521–6539.

<https://doi.org/10.1007/s13369-022-07401-4>

40. Kotowski, A. (2016). THE METHOD OF FREQUENCY DETERMINATION OF IMPULSE RESPONSE COMPONENTS BASED ON CROSS-CORRELATION VS. FAST FOURIER TRANSFORM, *17*(1), 59–64.
41. Popardovský, V., Ferenčák, M., Kriš, T., Tomašík, M., & Novotný, L. (2021). Tricopter vibration analysis. *Diagnostyka*, *22*(3), 67–72. <https://doi.org/10.29354/DIAG/141314>
42. Al-Haddad, L. A., Jaber, A. A., Neranon, P., & Al-Haddad, S. A. (2023). Investigation of Frequency-Domain-Based Vibration Signal Analysis for UAV Unbalance Fault Classification. *Engineering and Technology Journal*, *41*(7), 1–9. <https://doi.org/10.30684/etj.2023.137412.1348>
43. Yao, Y., Li, X., Yang, Z., Li, L., Geng, D., Huang, P., ... Song, Z. (2022). Vibration Characteristics of Corn Combine Harvester with the Time-Varying Mass System under Non-Stationary Random Vibration. *Agriculture (Switzerland)*, *12*(11). <https://doi.org/10.3390/agriculture12111963>
44. Oyarzun, J., Aizpuru, I., & Baraia-Etxaburu, I. (2022). Time–Frequency Analysis of Experimental Measurements for the Determination of EMI Noise Generators in Power Converters. *Electronics (Switzerland)*, *11*(23). <https://doi.org/10.3390/electronics11233898>
45. Noureddine, L., Noureddine, M., Hafaifa, A., & Kouzou, A. (2019). DWT-PSD extraction feature for defect diagnosis of small wind generator. *Diagnostyka*, *20*(3), 45–52. <https://doi.org/10.29354/diag/110458>
46. Jaber, A. A., & Bicker, R. (2018). Development of a condition monitoring algorithm for industrial robots based on artificial intelligence and signal processing techniques. *International Journal of Electrical and Computer Engineering*, *8*(2), 996–1009. <https://doi.org/10.11591/ijece.v8i2.pp996-1009>
47. Ravikumar, K. N., Madhusudana, C. K., Kumar, H., & Gangadharan, K. V. (2022). Classification of gear faults in internal combustion (IC) engine gearbox using discrete wavelet transform features and K star algorithm. *Engineering Science and Technology, an International Journal*, *30*. <https://doi.org/10.1016/j.jestch.2021.08.005>
48. Hazeri, H., Zarjam, P., & Azemi, G. (2021). Classification of normal/abnormal PCG recordings using a time–frequency approach. *Analog Integrated Circuits and Signal Processing*, *109*(2), 459–465. <https://doi.org/10.1007/s10470-021-01867-2>
49. Chikkam, S., & Singh, S. (2023). Condition Monitoring and Fault Diagnosis of Induction Motor using DWT and ANN. *Arabian Journal for Science and Engineering*, *48*(5), 6237–6252. <https://doi.org/10.1007/s13369-022-07294-3>
50. Al-Haddad, L. A., & Jaber, A. A. (2023). An intelligent fault diagnosis approach for multirotor UAVs based on deep neural network of multi-resolution transform features. *Drones*, *7*(2), 82. <https://doi.org/10.3390/drones7020082>
51. A. R. Mohanty, *Machinerycondition Monitoring: Principles And Practices*: Taylor & Francis Group, 2015. (n.d.). <https://doi.org/10.1201/9781351228626>
52. Li, B., Jiang, Z., & Chen, J. (2022). Performance of the Multiscale Sparse Fast Fourier Transform Algorithm. *Circuits, Systems, and Signal Processing*, *41*(8), 4547–4569. <https://doi.org/10.1007/s00034-022-01989-6>
53. Ardolino, R. S. (2007). *Wavelet-based signal processing of electromagnetic pulse generated waveforms*. NAVAL POSTGRADUATE SCHOOL MONTEREY CA.
54. Jawad, S. M., & Jaber, A. A. (2023). Bearings Health Monitoring Based on Frequency-Domain Vibration Signals Analysis. *Engineering and Technology Journal*, *41*(01), 86–95. <https://doi.org/10.30684/etj.2022.131581.1043>
55. Gonçalves, M. A., Gonçalves, A. S., Franca, T. C. C., Santana, M. S., da Cunha, E. F. F., & Ramalho, T. C. (2022). Improved Protocol for the Selection of Structures from Molecular Dynamics of Organic Systems in Solution: The Value of Investigating Different Wavelet Families. *Journal of Chemical Theory and Computation*, *18*(10), 5810–5818. <https://doi.org/10.1021/acs.jctc.2c00593>
56. Too, J., Abdullah, A. R., Mohd Saad, N., Mohd Ali, N., & Musa, H. (2018). A detail study of wavelet families for EMG pattern recognition. *International Journal of Electrical and Computer Engineering*, *8*(6), 4221–4229. <https://doi.org/10.11591/ijece.v8i6.pp.4221-4229>
57. S. Rajbhandari, “Application of Wavelets and Artificial Neural Network for Indoor Optical Wireless Communication Systems”, PhD Thesis, School of Computing, Engineering and Information Sciences, University of Northumbria at Newcastle, UK, 2009. (n.d.).
58. D. Giaouris, B. Zahawi, G. El-Murr, and V. Pickert, “Application of Wavelet Transformation for the Identification of High Frequency Spurious Signals in Step Down DC - DC Converter Circuits Experiencing Intermittent Chaotic Patterns,” in *Power Electronics, Machines and Drives*, 2006. The 3rd IET International Conference on, 2006, pp. 394-397. (n.d.). <https://doi.org/10.1049/cp:20060138>

59. Ong, P., Tieh, T. H. C., Lai, K. H., Lee, W. K., & Ismon, M. (2019). Efficient gear fault feature selection based on moth-flame optimisation in discrete wavelet packet analysis domain. *Journal of the Brazilian Society of Mechanical Sciences and Engineering*, 41(6), 266. <https://doi.org/10.1007/s40430-019-1768-x>
60. Vivas, E. L. A., Garcia-Gonzalez, A., Figueroa, I., & Fuentes, R. Q. (2013). Discrete Wavelet transform and ANFIS classifier for Brain-Machine Interface based on EEG. In *2013 6th International Conference on Human System Interactions, HSI 2013* (pp. 137–144). <https://doi.org/10.1109/HSI.2013.6577814>
61. Stanković, M., Mirza, M. M., & Karabiyik, U. (2021). UAV forensics: DJI mini 2 case study. *Drones*, 5(2), 49. <https://doi.org/10.3390/drones5020049>
62. Yang, C.-C., Chuang, H., & Kao, D.-Y. (2021). Drone Forensic Analysis Using Relational Flight Data: A Case Study of DJI Spark and Mavic Air. *Procedia Computer Science*, 192, 1359–1368. <https://doi.org/https://doi.org/10.1016/j.procs.2021.08.139>
63. Al-Haddad, L. A., & Jaber, A. A. (2022). An Intelligent Quadcopter Unbalance Classification Method Based on Stochastic Gradient Descent Logistic Regression. In *2022 3rd Information Technology To Enhance e-learning and Other Application (IT-ELA)* (pp. 152–156). <https://doi.org/10.1109/IT-ELA57378.2022.10107922>
64. Jaber, A. A., & Bicker, R. (2014). A simulation of non-stationary signal analysis using wavelet transform based on LabVIEW and Matlab. In *Proceedings - UKSim-AMSS 8th European Modelling Symposium on Computer Modelling and Simulation, EMS 2014* (pp. 138–144). Institute of Electrical and Electronics Engineers Inc. <https://doi.org/10.1109/EMS.2014.38>
65. H. Hadi, M., Hussain Issa, A., & Alaa Sabri, A. (2021). Design and FPGA Implementation of Intelligent Fault Detection in Smart Wireless Sensor Networks. *Engineering and Technology Journal*, 39(4A), 653–662. <https://doi.org/10.30684/etj.v39i4A.1951>
66. Ghermoul Oussama and Benguesmia, H. and B. L. (2023). Finite element modeling for electric field and voltage distribution along the cap and pin insulators under pollution. *Diagnostyka*, 24(2), 1–9. <https://doi.org/10.29354/diag/159517>
67. Flaieh, E. H., Hamdoon, F. O., & Jaber, A. A. (2020). Estimation the natural frequencies of a cracked shaft based on finite element modeling and artificial neural network. *International Journal on Advanced Science, Engineering and Information Technology*, 10(4), 1410–1416. <https://doi.org/10.18517/ijaseit.10.4.12211>
68. Ogaili, A. A. F., Hamzah, M. N., & Jaber, A. A. (2022). Integration of Machine Learning (ML) and Finite Element Analysis (FEA) for Predicting the Failure Modes of a Small Horizontal Composite Blade. *International Journal of Renewable Energy Research (IJRER)*, 12(4), 2168–2179.
69. Sheng, T. K., Esakki, B., Ganesan, S., & Salunkhe, S. (2019). Finite element analysis, prototyping and field testing of amphibious UAV. *UPB Sci. Bull. Ser. D Mech. Eng*, 81, 125–140.
70. Guan, Y., Xu, W., & Zhang, M. (2020). Nonlinear modeling of composite wing with application to UAV flight dynamic analysis. *Mechanical Systems and Signal Processing*, 138, 106542. <https://doi.org/https://doi.org/10.1016/j.ymssp.2019.106542>
71. Harnefors, L., Finger, R., Wang, X., Bai, H., & Blaabjerg, F. (2017). VSC Input-Admittance Modeling and Analysis Above the Nyquist Frequency for Passivity-Based Stability Assessment. *IEEE Transactions on Industrial Electronics*, 64(8), 6362–6370. <https://doi.org/10.1109/TIE.2017.2677353>
72. Pietrzak, P., & Wolkiewicz, M. (2023). Demagnetization Fault Diagnosis of Permanent Magnet Synchronous Motors Based on Stator Current Signal Processing and Machine Learning Algorithms. *Sensors*, 23(4). <https://doi.org/10.3390/s23041757>
73. Gao, A., Feng, Z., & Liang, M. (2021). Permanent magnet synchronous generator stator current AM-FM model and joint signature analysis for planetary gearbox fault diagnosis. *Mechanical Systems and Signal Processing*, 149, 107331. <https://doi.org/https://doi.org/10.1016/j.ymssp.2020.107331>
74. Yu, J., Wang, S., Wang, L., & Sun, Y. (2023). Gearbox fault diagnosis based on a fusion model of virtual physical model and data-driven method. *Mechanical Systems and Signal Processing*, 188, 109980. <https://doi.org/https://doi.org/10.1016/j.ymssp.2022.109980>
75. Gohshi, S. (2012). A new signal processing method for video: reproduce the frequency spectrum exceeding the Nyquist frequency. In *Proceedings of the 3rd Multimedia Systems Conference* (pp. 47–52).